ACS APPLIED MATERIALS & INTERFACES

www.acsami.org

Research Article

Alkali Halide Boost of Carbon Nitride for Photocatalytic H_2 Evolution in Seawater

Wenming Xu, Xuedong Zhao, Xianghui An, Sha Wang, Jing Zhang, Zishu Li, Wenting Wu,* and Mingbo Wu*

Cite This: *ACS Appl. Mater. Interfaces* 2020, 12, 48526−48532

Read Online

ACCESS | Metrics & More | Article Recommendations | Supporting Information

ABSTRACT: Photocatalytic H_2 evolution (PHE) from extremely abundant seawater resources is an ideal way to secure sustainable H_2 for humanity, but the saline in seawater easily competitively absorbs the active sites and poisons the catalyst. Herein, a series of low-cost alkali halide (NaI, KI, RbI, CsI, CsBr, and CsCl), analogous to the saline in natural seawater, was selected to modify carbon nitride (MX-CN) through one-step facile pyrolysis with the assistance of water. MX-CN possesses a large amount of negative charges, which could inhibit anion absorption, to some extent, preventing chloride corrosion. Importantly, it can greatly boost the electron transfer between MX-CN and triethanolamine (TEOA) (sacrificial agent) because the alkali cation in seawater can coordinate with TEOA, and easily come in contact with MX-CN through alkali-cation exchange and electrostatic attraction. Benefiting from it, the PHE performance in seawater is 200 times better than that of original CN in deionized water above, and the apparent quantum efficiency of MX-CN (CsI-CN) under 420 nm light irradiation comes to 72% in seawater, the highest value reported for seawater thus far. This work provides a new research direction for engineering the electron transfer pathway between the photocatalyst and sacrificial agent (e.g., pollutant) in natural seawater.

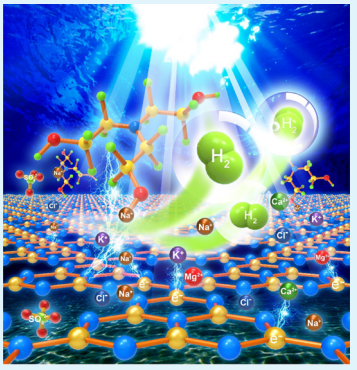

KEYWORDS: *carbon nitride, photocatalytic H_2 evolution, seawater, alkali halide, electron transfer*

1. INTRODUCTION

The shortage of fresh water resources and energy crisis are major challenges facing the world today. The actual use rate of seawater is very low, although which accounts for more than 97% of all water resources.[1−3] Hydrogen energy as a clean energy source can help solve the increasingly serious environmental pollution problems and energy crisis problems and is an ideal substitute for various fossil fuels.[4−6] Therefore, it is an impactful quest to utilize seawater and solar energy, readily available resources, to secure sustainable H_2 for humanity. Containing large amounts of various salts is the characteristic feature of seawater, mainly including Na^+, Mg^{2+}, Ca^{2+}, K^+, Cl^-, and SO_4^{2-}, which make up >90% of the total salt content of seawater.[7] The presence of these salts actually influences the photocatalysis, wherein most of the photocatalysts in natural or simulated seawater show lower efficiency than those in pure water,[8−11] while only a few cases show the opposite performance.[12] The poor performance is possible that the competitive absorption of salts on active sites inhibits sacrificial agent absorption.[13,14] Despite the considerable advances realized, the photocatalyst for H_2 evolution remains confined to the conventional design methods that are generally used in pure water, thus reinforcing the need for a change in the strategy.

Carbon nitride (CN) polymers are optimal photocatalytic materials,[15−19] and their surface structure and electronic properties are feasibly tuned using inorganic and organic synthesis methods,[20−23] which provide CN great opportunities to utilize the saline in seawater and to promote their photocatalysis performance. CN possessing large negative charge can inhibit anion absorption (e.g., Cl^-), to some extent, preventing chloride corrosion.[24,25] At the same time, cation ions (e.g., Na^+) have a tendency to attach a sacrificial agent with −OH groups through ionic bonds or electrostatic interactions, forming Na^+−sacrificial agent coordination.[26] It is speculated that CN with large negative charge can easily adsorb cation ions (e.g., Na^+-TEOA). The effective adsorption of the sacrificial agent onto the surface of the photocatalyst can react more efficiently with the holes generated by the light, to a great extent, prohibiting electron−hole recombination and subsequently improving the electron transfer of photocatalysis.

In this work, we have selected alkali halide salts (inorganic methods, analogous to the saline in natural seawater) to modify the graphite-phase CN with the assistance of a small amount of water through a further facile calcination. This method simultaneously modifies the surface structure (poly(heptazine

Received: July 20, 2020
Accepted: September 30, 2020
Published: October 13, 2020

Downloaded via CHINA UNIV OF PETROLEUM on November 8, 2020 at 07:45:34 (UTC).
See https://pubs.acs.org/sharingguidelines for options on how to legitimately share published articles.

ACS Publications

© 2020 American Chemical Society

https://dx.doi.org/10.1021/acsami.0c13060
ACS Appl. Mater. Interfaces 2020, 12, 48526−48532

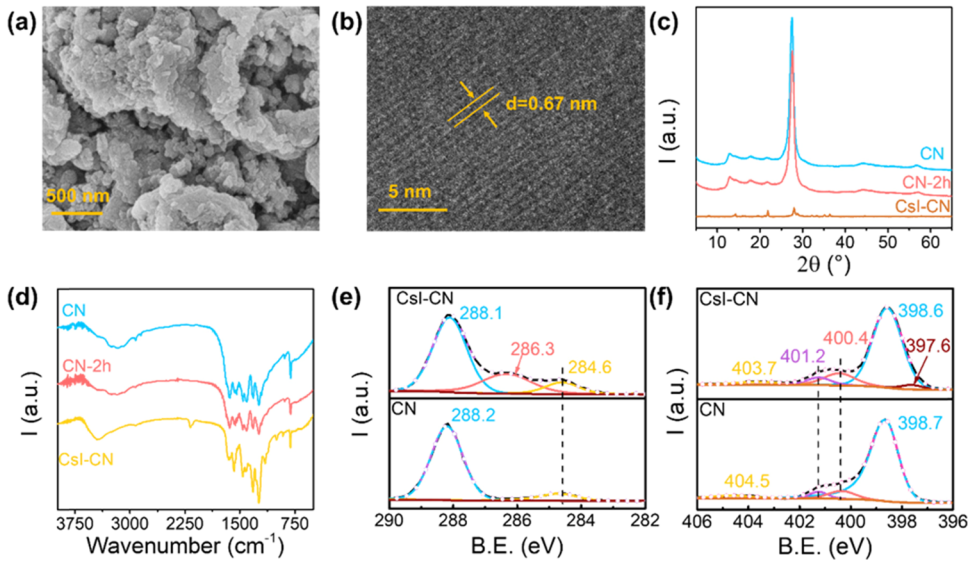

Figure 1. (a) SEM and (b) TEM images of CsI-CN, (c) comparative XRD patterns and (d) FT-IR spectra of the samples, and high-resolution (e) C 1 s and (f) N 1 s XPS of the samples.

imides) (PHI)) crystal phase with more hydroxyl groups and a large negative charge, which improves the hydrophilicity and electron transfer properties of CN itself. Interestingly, the saline in the seawater shows enhanced photocatalytic H_2 evolution (PHE) activity, with the highest H_2 evolution of 46.38 μmol (200 times higher than that of original CN in deionized water) and 72% apparent quantum efficiency (AQE) under 420 nm light irradiation (Equation S1). The synergies of the cation ions, sacrificial agent, and modified CN were studied by experimental analysis to gain molecular understanding of the prominent PHE activity boosted by seawater.

2. EXPERIMENTAL SECTION

2.1. Alkali Halide Assisted the Preparation of CN. Dicyandiamide (10 g) was thoroughly ground in a mortar and then transferred to a quartz boat. The quartz boat was wrapped in aluminum foil and placed in a tube furnace. The temperature was raised to 550 °C at a heating rate of 2.3 °C/min under a nitrogen atmosphere for 4 h, and the pale yellow bulk phase g-C_3N_4 was obtained after natural cooling. These bulk solids were thoroughly ground and collected for use. The resultant product was denoted as CN.

CN (500 mg) was placed in a mortar, and a total amount of 0.2 mL of deionized water was added drop by drop during the grinding. After fully grinding, the mixture was added to 1000 mg of alkali halide salts and ground again. Then, the mixture was transferred to a tube furnace with a corundum boat and heated to 550 °C for 2 h with a ramp rate of 5 °C/min under a nitrogen atmosphere. After cooling to room temperature, the product was further ground and ultrasonically dispersed in deionized water. Finally, it was washed with deionized water by centrifugation several times and dried at 60 °C overnight. The sample was denoted as MX-CN (M represents alkali and X represents halide salts), depending on the kinds of alkali and halogens added. In addition, NaI-assisted CN was only heated for 1 h because as the heating time was prolonged to 2 h, no CN was obtained, only leaving white crystal salt.

For comparison, CN was ground fully and further heated to 550 °C for 2 h under the same conditions, which was referred to as CN-2 h.

2.2. Characterization. The samples were characterized by X-ray diffraction (XRD) (X'Pert PRO MPD, Holland), scanning electron microscopy (SEM) (Hitachi SU8010, Japan), Fourier transform infrared spectrometry (FT-IR) (Thermo Nicolet NEXUS670, USA), and X-ray photoelectron spectroscopy (XPS) using a Kratos AXIS Ultra spectrometer equipped with a prereduction chamber and an Elementar Vario EL III instrument (Elementar, Germany). The UV−vis diffuse reflectance spectra were obtained from the dry-pressed disk samples using a Scan UV−vis spectrophotometer (UV−vis DRS UV-2700, Shimadzu, Japan) equipped with an integrating sphere assembly, using $BaSO_4$ as a reflectance sample. Time-resolved fluorescence decay spectra were obtained using an Edinburgh FLS980 spectrophotometer with an excitation wavelength of 380 nm and an emission wavelength of 450 nm. Photoluminescence (PL) spectra were measured on a fluorospectrophotometer (F97pro, Lengguang Tech, China). A Malvern Zetasizer Nano ZS90 nanometer particle size potentiometer was used to test various kinds of CN and determine the charge size on its surface.

2.3. Photocatalytic Hydrogen Activity Test. PHE was performed as follows. The catalyst powder (4 mg) was dispersed in 4 mL aqueous solution (natural seawater, simulated seawater, or deionized water) containing 10 vol % triethanolamine (TEOA) scavengers flushed with Ar gas. Pt (2 wt %) was loaded on the surface of the photocatalyst as a cocatalyst using an in situ photodeposition method with K_2PtCl_6. The solution was then irradiated with a 300 W xenon lamp equipped with a 420 nm cutoff filter at room temperature. The concentration of hydrogen gas in a headspace was quantified using a Shimadzu GC-2014 gas chromatograph [Ar carrier, a capillary column with molecular sieves of 5A] equipped with a thermal conductivity detector.

In addition, the positive and negative charges of simulated seawater were equal to those of 3.5 wt % NaCl, which were calculated based on the same molar concentration. Unlike a previous report with desalination treatment,[27] the natural seawater in this work was directly obtained from the Yellow Sea and the South China Sea through simple filtration (0.22 μm filter) to remove some algae, microorganisms, and solid particles present.

3. RESULTS AND DISCUSSION

3.1. Morphology and Chemical Structure Characterization. After alkali halide and water modification, the morphology and structure of MX-CN were studied. Most of the MX-CN samples show a regular lattice structure, which was studied by SEM and transmission electron microscopy (TEM) as shown in Figure S1. As a representative, CsI-CN is shown in Figure 1a,b. Compared with CN, the SEM image of CsI-CN shows uniform grain accumulation, and the most obvious change of the TEM image is the occurrence of lattice fringes. The mapping images in Figure S2 show that the elements of CsI-CN are uniformly distributed based on the modification of both

https://dx.doi.org/10.1021/acsami.0c13060
ACS Appl. Mater. Interfaces 2020, 12, 48526−48532

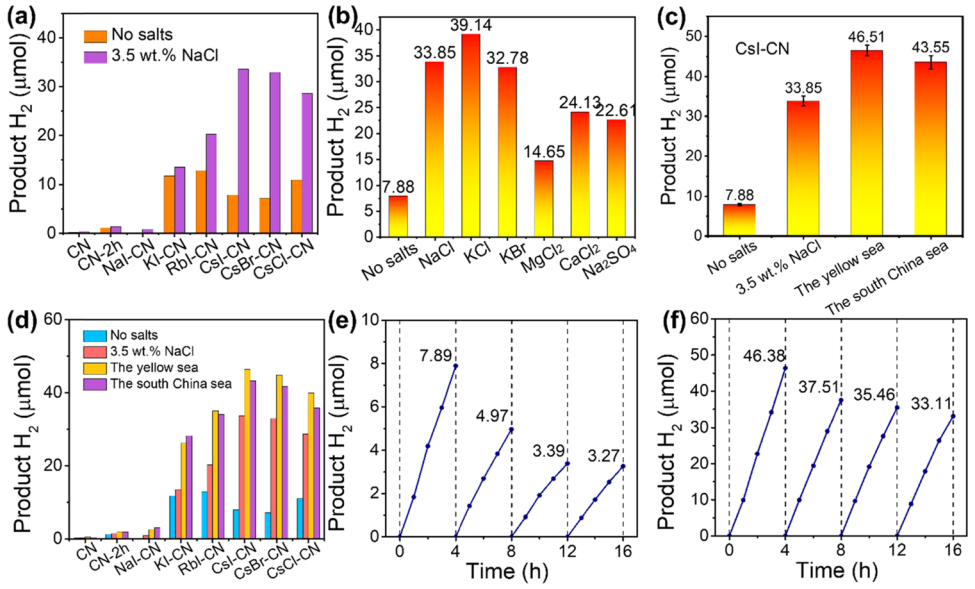

Figure 2. (a) Product H_2 for samples in the first 4 h with 3.5 wt % NaCl solution or deionized water. (b) Product H_2 for CsI-CN in the presence of other salts with a positive and negative charge equal to that of 3.5 wt % NaCl for 4 h (by default all salts completely disassociate). (c) Product H_2 for CsI-CN in the first 4 h with deionized water, 3.5 wt % NaCl solution (simulated seawater), the Yellow Sea, or the South China Sea. (d) Product H_2 for samples in the first 4 h with deionized water, 3.5 wt % NaCl solution, the Yellow Seawater, or the South China Seawater. (e) Cycling stability test of CsI-CN with deionized water. (f) Cycling stability test of CsI-CN with the Yellow Sea water. Reaction conditions: 4 mg samples, visible light irradiation ($\lambda >$ 420 nm), TEOA (10 v.%) as the sacrificial agent, and Pt (2 wt %) as the cocatalyst.

CsI and a little water. This shows that alkali halides can improve the order degree of CN, reducing the defect sites where electron−hole pairs recombine.[28] The XRD patterns (Figure 1c) indicate that CsI-CN has a PHI crystal phase.[29] This indicates that CsI could destroy the part of the heptazine ring of CN. The H, C, and N elemental contents of the samples were further tested by elemental analysis to verify the PHI crystal phase, as shown in Table S1. The n(C)/n(N) ratio value of the salt-modified CN is significantly increased and is closer to the value of the PHI structure (0.71).[30] Other modified MX-CN samples are similar to CsI-CN showing a crystal phase PHI structure (Figure S3). The structure of PHI will make it easier for CN to coordinate with the ions in the seawater.[12] The specific surface area of the samples is presented in Table S6.

The functional groups can provide the alkali chelation sites and influence the electron densities of MX-CN. As shown in Figure 1d and Figure S4, all samples in FT-IR spectra have a characteristic peak of CN, a respiratory vibration peak of a triazine ring at 810 cm^{-1}, and a stretching vibration peak of tri-s-triazine of 1200−1650 cm^{-1}.[31] The broad absorption band at 2400−3650 cm^{-1} indicates the presence of hydroxyl groups, adsorbed water, and terminal amino groups on the surface of samples.[21] Compared with CN, the salt-modified CN showed a new absorption peak at 2178 cm^{-1}, which is the absorption peak of the terminal cyano group (C≡N),[32] indicating that the alkali halide can modify the CN structural unit. In addition, the absorption bands at 996 and 1156 cm^{-1} are due to the symmetric and asymmetric vibrations of NC_2 bonds and metal−NC_2 groups, respectively.[29] From another perspective, −NC_2 functional groups provide alkali metal-chelated sites.

Then, XPS was used to analyze the surface chemical properties of samples (Figure S5). Although CN was modified by alkali halides, the elemental content of alkali metal comes to 5−7 atm.%, but the halide element content of iodine is only 0.1−0.3 atm.% (Table S2). As shown in the high-resolution C1s XPS of CN and CsI-CN (Figure 1e), CsI-CN shows a new signal peak at 286.3 eV assigned to the signal C−OH carbon when compared to CN.[29] This is also consistent with the fact that the oxygen element content (6.09 atm.%) of CsI-CN (Table S2) is significantly higher than that of CN (2.37 atm.%). The increase of hydroxyl groups is beneficial to enhancing the hydrophilic properties of the photocatalyst. In the high-resolution N 1 s XPS of CN and CsI-CN (Figure 1f), there are four signal peaks for CN at 398.7, 400.0, 401.2, and 404.5 eV, respectively, which are sequentially assigned to the tri-s-triazine ring C−N=C nitrogen, $N(C)_3$ nitrogen, incompletely polymerized $-NH_2$ or −NH nitrogen, and charge effects.[33] Compared to CN, CsI-CN has a new negatively shifted peak at 397.6 eV, which can be assigned to the deprotonated nitrogen N^{Θ}.[29] The deprotonated nitrogen N^{Θ} could make the photocatalyst easier to adsorb and coordinate with ions in seawater. In addition, the binding energy of part of carbon and nitride of CsI-CN is shifted to a low value, indicating that their electron densities are increasing. The C 1 s and N 1 s XPS of the other samples modified by other alkali halide salts are similar to those of CsI-CN (Figure S6).

Based on the analysis mentioned above, the alkali halide-modified CN has a PHI crystal phase structure; at the same time, it was decorated with hydroxyl groups, alkali cations, and deprotonated nitrogen N^{Θ}, which can coordinate or exchange with alkali cations in the seawater. These modifications change the carrier transfer capability and electron density distribution of CN and will be more favorable for the directional migration of photogenerated electrons and holes, thereby promoting the photocatalytic reaction.

In addition, the optical properties of the samples were characterized using diffuse reflectance spectra (Figure S7−S10), PL spectra (Figure S11), and time-resolved PL spectra (Figure S12). The ability of samples to transmit photogenerated carriers was tested by the transient photocurrent response and electrical impedance spectra (Figure S13). The results indicate that MX-CN has more excellent photogenerated electron and hole

https://dx.doi.org/10.1021/acsami.0c13060
ACS Appl. Mater. Interfaces 2020, 12, 48526−48532

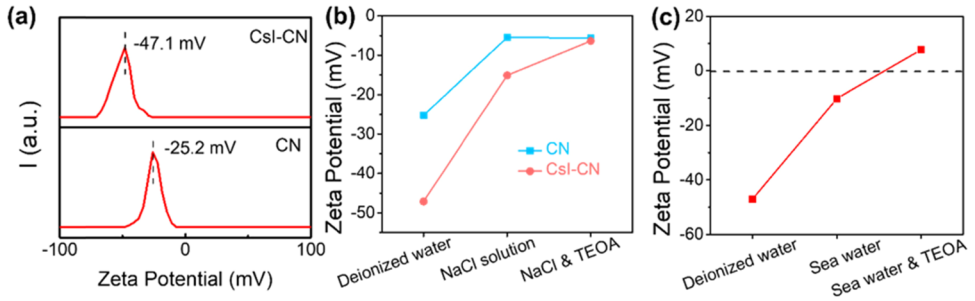

Figure 3. (a) Zeta potential of CN and CsI-CN. (b) Zeta potential change curves of CN and CsI-CN in deionized water, NaCl solution, and NaCl solution containing TEOA. (c) Zeta potential change curves of CsI-CN in deionized water, seawater, and seawater solution containing TEOA. Notes: The concentration of NaCl solution was 3.5 wt %, and the concentration of TEOA was 10 v%. Before the zeta potential test, all samples were dispersed and stirred for 30 min to achieve adsorption equilibrium.

transporting ability and is more advantageous for the PHE reaction.

3.2. PHE in Seawater. To study the structure−activity relationship, MX-CN was first applied to PHE in pure water and simulated seawater (3.5 wt % NaCl), respectively. The saline in simulated seawater can improve the PHE productivity of all these catalysts, especially for the alkali halide-modified MX-CN (Figure 2a). For example, the amount of hydrogen in the first 4 h of CsI-CN reached 33.62 μmol, which is four times more than that of itself in deionized water (7.89 μmol), 120 times that of CN in simulated seawater (0.27 μmol), and 187 times that of CN in deionized water (0.18 μmol). Considering the existence of various ions (major ions: Na^+, Mg^{2+}, Ca^{2+}, K^+, Cl^-, and SO_4^{2-}, making up >90% of the total salt content of seawater) in natural seawater,[7,34] the PHE of CsI-CN as a representative sample was studied in saline solution (e.g., NaCl, KCl, KBr, $MgCl_2$, $CaCl_2$, and Na_2SO_4). In Figure 2b, it can be seen that both anions and cations have great positive effects on the PHE of CsI-CN, with different enhancing extents. For the PHE application, this demonstrates that MX-CN is more adaptable to a wide range of saline with great qualities.

Taking into account the complexity components of natural seawater, two kinds of seawater were collected from the South China Sea (Shenzhen, China) and the Yellow Sea (Dalian, China) to test the PHE performance. The major ion content of these two natural seawater samples was determined by ion chromatography, as shown in Table S3. Before the test, the seawater used in the reaction only needs to be simply filtered through a 0.220 μm filter to remove microorganisms, algae, and solid particles from seawater. Figure 2c shows the PHE productivity of CsI-CN in deionized water, simulated seawater, the Yellow Sea, and the South China Sea. In the case of the Yellow Sea, the hydrogen production of the first 4 h is 46.51 μmol, which is 5.9 times that of the sample in deionized water (7.88 μmol) and 258 times that of CN in deionized water (0.18 μmol) (Figure S14). The AQE at 420 nm light irradiation could reach 72%, the highest value reported for seawater thus far (Table S4). Other samples show similar results for the PHE productivity (Figure 2d) fully confirming that MX-CN is more suitable to natural seawater. To some extent, the PHE productivity of MX-CN in natural seawater is better than that in simulated seawater.

The comparisons of the PHE cycling stability were further studied in both deionized water and the Yellow Sea (Figure 2e). After the first cycle, the hydrogen production of CsI-CN in deionized water decreased significantly from 7.89 to 4.97 μmol, a decrease coming to 63.0%. This downward trend almost stopped by the ending of the third cycle with a decrease to 43.0%. For CsI-CN in the Yellow Seawater (Figure 2f), there is a small decrease from 46.38 to 37.51 μmol after the first cycle followed by a slight gradual descent. The hydrogen production in the fourth cycle was 33.11 μmol, which was 71.4% of the first cycle. Furthermore, compared with the hydrogen production of the first 4 h of CN (0.18 μmol), the hydrogen production of Cs-CN in the fourth cycle is still 184 times higher than that of CN. Therefore, the seawater can not only enhance the PHE performance but also greatly promote the stability of MX-CN.

3.3. Mechanism of Photocatalytic Seawater Hydrogen Evolution. In this part, CsI-CN was selected as a representative to study the mechanism of PHE in seawater. Given the abundant ions in seawater, the increasing PHE activity of MX-CN is likely due to the interaction between the surface of the photocatalyst and the ions in seawater. Therefore, the surface charge of the sample was first tested by zeta potential. Figure 3a shows a comparison of the zeta potential curves of CsI-CN and CN (CN needs to wash off the unpolymerized precursor with hot water and be dried before testing). The zeta potential of CsI-CN reached −47.1 mV, which was −21.9 mV negative shifting compared to that of CN (−25.2 mV). This indicates the increasing amount of negative charge on the surface of CsI-CN, which is more advantageous for adsorbing cations in the seawater.

To prove that MX-CN can adsorb ions in seawater, the zeta potential of the CsI-CN under different aqueous conditions was further tested and compared with that of CN. As shown in Figure 3b, the zeta potentials of CN and CsI-CN in simulated seawater were reduced to −5.5 mV and − 15.1 mV, respectively, indicating that CN and CsI-CN are capable of adsorbing cations in salt solutions because of the negative charge on the photocatalyst surface. Interestingly, in the simulated seawater containing TEOA, the zeta potential of CN is almost unchanged (−5.6 mV), while the zeta potential of CsI-CN continues to decrease to −6.4 mV. According to the literature, Na^+ can adsorb the sacrificial agent, forming Na−sacrificial agent coordination,[26] which is Na-TEOA in this work. Therefore, it may be due to the small amount of charge carried by CN itself, which mainly adsorbs free Na^+ and is difficult to adsorb Na-TEOA, while CsI-CN can adsorb both Na^+ and Na-TEOA because of its relatively large electronegativity.

In addition, the zeta potential of CsI-CN in seawater and seawater containing TEOA was tested, as shown in Figure 3c. It can be seen that the zeta potential of CsI-CN is −10.2 mV in seawater solution and 7.7 mV, a positive potential, in seawater containing TEOA. Because of the alkaline properties of TEOA

https://dx.doi.org/10.1021/acsami.0c13060
ACS Appl. Mater. Interfaces 2020, 12, 48526−48532

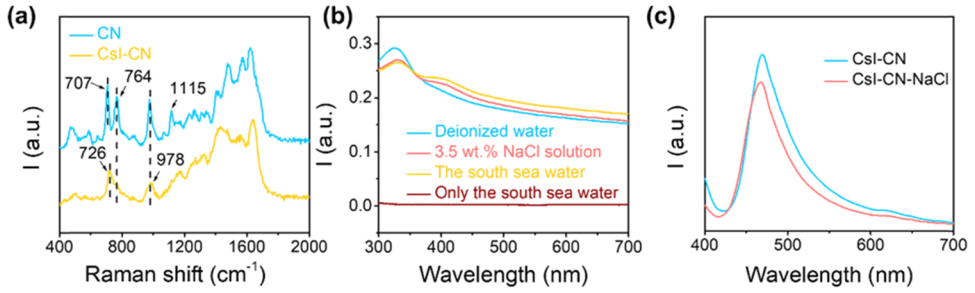

Figure 4. (a) Raman spectra (325 nm excitation) of CN and CsI-CN. (b) UV−vis absorbance spectra of seawater and CsI-CN solution under different conditions. Before the UV−vis absorbance spectra test, all samples were dispersed and stirred for 30 min to achieve adsorption equilibrium. (c) Fluorescence spectra of CsI-CN and CsI-CN added to a small amount of NaCl solution. This NaCl solution contains 3.5 wt % NaCl and 10 v% TEOA. Notes: Before the UV−vis absorbance spectra test, all samples were dispersed and stirred for 30 min to achieve adsorption equilibrium

Table 1. Elemental Composition from XPS for Analyzing the Surface Change before and after the Reaction[a]

samples	C atm.%	N atm.%	O atm.%	Cs atm.%	I atm.%	Na atm.%	Cl atm.%	Pt atm.%
CsI-CN	42.96	45.44	6.09	5.24	0.28			
R-CsI-CN	48.81	38.09	10.39	1.76	0.13			0.83
R-CsI-CN-NaCl	52.66	28.12	14.83	0.18	0.15	3.45	0.53	0.08

[a]Note: R-CsI-CN and R-CsI-CN-NaCl represent the samples obtained by centrifugation of CsI-CN in deionized water and simulated seawater after reacting for 4 h, respectively.

aqueous solution, it means that TEOA is more likely to release OH^-, and TEOA itself possesses positive potential. Then, Na^+ may be chelated with another hydroxyl of positive TEOA followed by the adsorption on the CsI-CN. Other cations (e.g., K^+, Mg^{2+}, Ca^{2+}, etc.) in the sea can also play similar roles to Na^+. The larger the variation value between the solutions with and without TEOA, the higher the absorbed TEOA amount. Therefore, the synergies of various salt ions in natural seawater help CsI-CN to absorb more TEOA.

Both CN and CsI-CN can adsorb and coordinate with Na^+ and Na-TEOA, but the PHE productivity of CsI-CN was improved greatly after CN was modified by CsI. For this, Raman spectra of CsI-CN and CN at 325 nm excitation were tested to explain this great PHE improvement. Figure 4a shows that CN has three distinct peaks at 707, 764, and 978 cm^{-1}. The peak at 978 cm^{-1} is the respiratory characteristic peak of the tri-s-triazine unit, and the other two peaks at 707 and 764 cm^{-1} are doubly degenerate vibrations associated with the in-plane bending vibration of tri-s-triazine linkage linked by CN═C. The peak intensity of CsI-CN is reduced, and its peak is shifted from 707 to 726 cm^{-1}, indicating that there is a directed charge transfer between the tri-s-triazine ring and the Cs in CsI-CN.[35,36] This directed charge migration to the surface of the photocatalyst can suppress the recombination of photogenerated electrons and holes. The reserved hole can react rapidly with the sacrificial agent TEOA adsorbed on the surface of the material, making it easier for electrons to reduce hydrogen.

The optical properties (e.g., absorption ability and fluorescence properties) also confirmed the synergy effect when CsI-CN came in contact with salts and TEOA. The UV−vis absorption spectra of natural seawater and CsI-CN in different solutions are shown in Figure 4b. It is found that the absorption edge of CsI-CN appears slightly red-shifted in seawater compared to that in deionized water and simulated seawater, which may be due to the charge transfer from the absorbed alkali ions in seawater to the CN.[37−39] The fluorescence spectrum of CsI-CN was also tested after adding a small amount of NaCl solution and 10 v% TEOA (Figure 4c). Compared with CsI-CN, the fluorescence intensity of CN containing NaCl solution became lower, indicating that the recombination of photogenerated electrons and holes can be suppressed to some extent when it adsorbed ions. In addition, the time-resolved PL spectra of samples (Figure S12) were tested. The fluorescence lifetime of MI-CN follows this trend NaI-CN > KI-CN > RbI-CN > CsI-CN, implying that the relaxation of a small fraction of MI-CN excitons occurs via nonradiative paths, presumably by charge transfer of electrons and holes with high mobility to new localized states.[40]

It is worth mentioning that the stability of CsI-CN in seawater is much better than that in deionized water. To find out the reason, XPS of CsI-CN reacting for 4 h in deionized water (R-CsI-CN) and artificial seawater (R-CsI-CN-NaCl) were tested (Table 1). For the comparison of R-CsI-CN and CsI-CN, it is found that the Cs element on the CN lost 66.4% after 4 h reaction in deionized water, which may be the main reason for the sharp decline in hydrogen evolution ability.[41] It is also found that the content of C and O of R-CsI-CN-NaCl is significantly higher than that of R-CsI-CN, while the content of the N element is obviously lower, just consistent with the adsorption of Na-TEOA on the CsI-CN surface in artificial seawater. At the same time, the detected Cs and Pt content of R-CsI-CN-NaCl is very low, about 10% of R-CsI-CN, mainly because Cs and Pt elements were covered by the adsorption of Na-TEOA, which protect Cs and Pt from shedding and subsequently stabilize its PHE performance.

Generally, the pH also has an influence on the PHE performance, so the pH of the mixed solution was tested under different conditions and is shown in Table S5. The pH of the mixture of TEOA and K_2PtCl_6 in deionized water is 10.94 (No.2), while this mixture in seawater increased to 9.78 (No.3). The pH of seawater is 7.89 (No.1), which is higher than that of deionized water, indicating that the complex components in seawater have a buffer function inhibiting TEOA to release OH^-. Comparing No. 2, 4, and 7, there is no pH change when the photocatalyst was used in deionized water. For No. 3, 6, and 9, the seawater has a little influence on the pH of the photocatalysis system, which may be because the saline in the

https://dx.doi.org/10.1021/acsami.0c13060
ACS Appl. Mater. Interfaces 2020, 12, 48526−48532

seawater can absorb onto the surface of the catalyst. For No. 8 and 10−13, various anions and cations also have an effect on pH in the photocatalysis system. Their synergies especially for the various saline solutions in seawater can enhance photocatalysis to some extent. In $MgCl_2$ solution (No.12), its pH is 9.01 lower than that of others, which may be because of the production of $MgOH_2$ precipitation. Generally speaking, the lower the pH, the better the PHE performance. It worth mentioning that the pH of CsI-CN in KCl solution is 10.69 (No. 11) close to that of CsI-CN in $CaCl_2$ (No.13, pH = 10.12, no precipitation), but the PHE performance of CsI-CN in KCl is 1.62 times that in $CaCl_2$. It indicates that the synergy of the alkali ions, sacrificial agent, and modified CN instead of pH is the key factor for the improved photocatalysis.

According to the above, alkali halide salt-modified CN with excellent PHE performance in seawater mainly benefits from the excellent properties of the modified materials and the interaction between the modified CN and salt ions in seawater, mainly including the adsorption of Na-TEOA and TEOA by the electronegative catalyst, the regulation of salt ions on pH of the hydrogen evolution reaction system, optimization of optical activity of the catalyst by the adsorption structure, and directional transfer of catalyst charge. The detailed mechanism process of the adsorption of Na-TEOA and TEOA by the electronegative catalyst is shown in Figure S15.

4. CONCLUSIONS

In summary, we developed CN (MX-CN) materials greatly adapted to the complex environment of natural seawater through a facile modification using both alkali halides and a tiny amount of water. The obtained MX-CN possesses a PHI crystal phase and functional groups such as alkali ions and the deprotonated nitrogen N^{Θ} on its surface, along with a more negative zeta potential, benefiting PHE. As confirmed, MX-CN can capture TEOA and Na-TEOA through alkali-cation exchange and electrostatic attraction and give a great boost to the separation of photogenerated carriers and the directional migration of the charge, which make MX-CN exhibit excellent photocatalytic seawater hydrogen evolution capability.

■ ASSOCIATED CONTENT

Supporting Information

The Supporting Information is available free of charge at https://pubs.acs.org/doi/10.1021/acsami.0c13060.

SEM and TEM images, Brunauer−Emmett−Teller surface areas, overpotential, FT-IR spectra, XPS, element contents, surface elemental composition, main ions and their contents in seawater, summary of the AQE for PHE in seawater, the pH of the solution under different conditions, the XRD of byproducts, zeta potential, diffuse reflectance spectra, PL spectra, time-resolved PL spectra, transient photocurrent response, the electronic band structure of samples, the cycling stability test of Cs-CN-2 h, and discussion of some experimental data (PDF)

■ AUTHOR INFORMATION

Corresponding Authors

Wenting Wu − *State Key Laboratory of Heavy Oil Processing, College of Chemical Engineering, China University of Petroleum (East China), Qingdao 266580, P. R. China;* orcid.org/0000-0002-8380-7904; Email: wuwt@upc.edu.cn

Mingbo Wu − *State Key Laboratory of Heavy Oil Processing, College of Chemical Engineering, China University of Petroleum (East China), Qingdao 266580, P. R. China;* orcid.org/0000-0003-0048-778X; Email: wumb@upc.edu.cn

Authors

Wenming Xu − *State Key Laboratory of Heavy Oil Processing, College of Chemical Engineering, China University of Petroleum (East China), Qingdao 266580, P. R. China*

Xuedong Zhao − *State Key Laboratory of Heavy Oil Processing, College of Chemical Engineering, China University of Petroleum (East China), Qingdao 266580, P. R. China*

Xianghui An − *State Key Laboratory of Heavy Oil Processing, College of Chemical Engineering, China University of Petroleum (East China), Qingdao 266580, P. R. China*

Sha Wang − *Jiangsu Provincial Key Laboratory of Pulp and Paper Science and Technology, Nanjing Forestry University, Nanjing 210037, China;* orcid.org/0000-0002-4906-8132

Jing Zhang − *State Key Laboratory of Safety and Control for Chemicals, SINOPEC Research Institute of Safety Engineering, Qingdao 266071, China*

Zishu Li − *Valiant Limited Company, Yeda 264006, China*

Complete contact information is available at: https://pubs.acs.org/10.1021/acsami.0c13060

Notes

The authors declare no competing financial interest.

■ ACKNOWLEDGMENTS

This study was financially supported by the National Key Research and Development Program of China (NO. 2019YFA0708700), the NSFC (51672309, 51172285, and 51372277), and the Fundamental Research Funds for Central Universities (18CX07009A). We also acknowledge the Young Taishan scholars program of Shandong province (tsqn20182027) and technological leading scholar of 10000 talent project (W03020508).

■ REFERENCES

(1) Rozema, J.; Flowers, T. Crops for a Salinized World. *Science* **2008**, *322*, 1478−1480.

(2) Khawaji, A. D.; Kutubkhanah, I. K.; Wie, J.-M. Advances in seawater desalination technologies. *Desalination* **2008**, *221*, 47−69.

(3) Tiwari, G. N.; Singh, H. N.; Tripathi, R. Present status of solar distillation. *Sol. Energy* **2003**, *75*, 367−373.

(4) Maeda, K. Photocatalytic water splitting using semiconductor particles: History and recent developments. *J. Photochem. Photobiol. C-Photochem. Rev.* **2011**, *12*, 237−268.

(5) Xu, Y.; Kraft, M.; Xu, R. Metal-free carbonaceous electrocatalysts and photocatalysts for water splitting. *Chem. Soc. Rev.* **2016**, *45*, 3039−3052.

(6) Momirlan, M.; Veziroglu, T. The properties of hydrogen as fuel tomorrow in sustainable energy system for a cleaner planet. *Int. J. Hydrogen Energy* **2005**, *30*, 795−802.

(7) Millero, F. J.; Feistel, R.; Wright, D. G.; McDougall, T. J. The composition of Standard Seawater and the definition of the Reference-Composition Salinity Scale. *Deep Sea Res. Part 1 Oceanogr Res. Pap* **2008**, *55*, 50−72.

(8) Li, Y.; He, F.; Peng, S.; Gao, D.; Lu, G.; Li, S. Effects of electrolyte NaCl on photocatalytic hydrogen evolution in the presence of electron donors over Pt/TiO_2. *J. Mol. Catal. A-Chem.* **2011**, *341*, 71−76.

(9) Li, Y.; He, F.; Peng, S.; Lu, G.; Li, S. Photocatalytic H_2 evolution from NaCl saltwater over $ZnS_{1-x-0.5y}O_x(OH)_y$−ZnO under visible light irradiation. *Int. J. Hydrogen Energy* **2011**, *36*, 10565−10573.

(10) Song, T.; Zhang, P.; Wang, T.; Ali, A.; Zeng, H. Constructing a novel strategy for controllable synthesis of corrosion resistant Ti^{3+} self-doped titanium−silicon materials with efficient hydrogen evolution activity from simulated seawater. *Nanoscale* **2018**, *10*, 2275−2284.
(11) Zhu, C.; Liu, C. A.; Fu, Y.; Gao, J.; Huang, H.; Liu, Y.; Kang, Z. Construction of CDs/CdS photocatalysts for stable and efficient hydrogen production in water and seawater. *Appl. Catal. B Environ.* **2019**, *242*, 178−185.
(12) Gao, H.; Yan, S.; Wang, J.; Zou, Z. Ion coordination significantly enhances the photocatalytic activity of graphitic-phase carbon nitride. *Dalton Trans.* **2014**, *43*, 8178−8183.
(13) Gao, M.; Connor, P. K. N.; Ho, G. W. Plasmonic photothermic directed broadband sunlight harnessing for seawater catalysis and desalination. *Energy Environ. Sci.* **2016**, *9*, 3151−3160.
(14) Krivec, M.; Dillert, R.; Bahnemann, D. W.; Mehle, A.; Štrancar, J.; Dražić, G. The nature of chlorine-inhibition of photocatalytic degradation of dichloroacetic acid in a TiO_2-based microreactor. *Phys. Chem. Chem. Phys.* **2014**, *16*, 14867−14873.
(15) Ghosh, I.; Khamrai, J.; Savateev, A.; Shlapakov, N.; Antonietti, M.; König, B. Organic semiconductor photocatalyst can bifunctionalize arenes and heteroarenes. *Science* **2019**, *365*, 360−366.
(16) Liu, J.; Liu, Y.; Liu, N.; Han, Y.; Zhang, X.; Huang, H.; Lifshitz, Y.; Lee, S.-T.; Zhong, J.; Kang, Z. Metal-free efficient photocatalyst for stable visible water splitting via a two-electron pathway. *Science* **2015**, *347*, 970−974.
(17) Wang, H.; Zhang, L.; Chen, Z.; Hu, J.; Li, S.; Wang, Z.; Liu, J.; Wang, X. Semiconductor heterojunction photocatalysts: design, construction, and photocatalytic performances. *Chem. Soc. Rev.* **2014**, *43*, 5234−5244.
(18) Lu, D.; Wang, H.; Zhao, X.; Kondamareddy, K. K.; Ding, J.; Li, C.; Fang, P. Highly Efficient Visible-Light-Induced Photoactivity of Z-Scheme g-C_3N_4/Ag/MoS_2 Ternary Photocatalysts for Organic Pollutant Degradation and Production of Hydrogen. *ACS Sustainable Chem. Eng.* **2017**, *5*, 1436−1445.
(19) Lin, X.; Du, S.; Li, C.; Li, G.; Li, Y.; Chen, F.; Fang, P. Consciously Constructing the Robust NiS/g-C_3N_4 Hybrids for Enhanced Photocatalytic Hydrogen Evolution. *Catal. Lett.* **2020**, *150*, 1898−1908.
(20) Wu, W.; Han, C.; Zhang, Q.; Zhang, Q.; Li, Z.; Gosztola, D. J.; Wiederrecht, G. P.; Wu, M. Functionalizing carbon nitride with heavy atom-free spin converters for enhanced $^1O_2$ generation. *J. Catal.* **2018**, *361*, 222−229.
(21) Wu, W.; Xu, W.; An, X.; Wang, L.; Zhang, J.; Li, Z.; Wu, M. Multiaspect insight into synergetic modification of carbon nitride with halide salt and water vapor. *Appl. Catal. B-Environ.* **2018**, *229*, 204−210.
(22) Wu, W.; Zhang, J.; Fan, W.; Li, Z.; Wang, L.; Li, X.; Wang, Y.; Wang, R.; Zheng, J.; Wu, M.; Zeng, H. Remedying Defects in Carbon Nitride To Improve both Photooxidation and H_2 Generation Efficiencies. *ACS Catal.* **2016**, *6*, 3365−3371.
(23) Zhang, J.; An, X.; Lin, N.; Wu, W.; Wang, L.; Li, Z.; Wang, R.; Wang, Y.; Liu, J.; Wu, M. Engineering monomer structure of carbon nitride for the effective and mild photooxidation reaction. *Carbon* **2016**, *100*, 450−455.
(24) Fukuzumi, S.; Lee, Y.-M.; Nam, W. Fuel Production from Seawater and Fuel Cells Using Seawater. *ChemSusChem* **2017**, *10*, 4264−4276.
(25) Kuang, Y.; Kenney, M. J.; Meng, Y.; Hung, W.-H.; Liu, Y.; Huang, J. E.; Prasanna, R.; Li, P.; Li, Y.; Wang, L.; Lin, M.-C.; McGehee, M. D.; Sun, X.; Dai, H. Solar-driven, highly sustained splitting of seawater into hydrogen and oxygen fuels. *Proc. Natl. Acad. Sci. U. S. A.* **2019**, *116*, 6624.
(26) Li, Y.; Gao, D.; Peng, S.; Lu, G.; Li, S. Photocatalytic hydrogen evolution over Pt/$Cd_{0.5}Zn_{0.5}S$ from saltwater using glucose as electron donor: An investigation of the influence of electrolyte NaCl. *Int. J. Hydrogen Energy* **2011**, *36*, 4291−4297.
(27) Ji, S. M.; Jun, H.; Jang, J. S.; Son, H. C.; Borse, P. H.; Lee, J. S. Photocatalytic hydrogen production from natural seawater. *J. Photochem. Photobiol. A-Chem.* **2007**, *189*, 141−144.
(28) Lin, L.; Ou, H.; Zhang, Y.; Wang, X. Tri-s-triazine-Based Crystalline Graphitic Carbon Nitrides for Highly Efficient Hydrogen Evolution Photocatalysis. *ACS Catal.* **2016**, *6*, 3921−3931.
(29) Chen, Z.; Savateev, A.; Pronkin, S.; Papaefthimiou, V.; Wolff, C.; Willinger, M. G.; Willinger, E.; Neher, D.; Antonietti, M.; Dontsova, D. "The Easier the Better" Preparation of Efficient Photocatalysts—Metastable Poly(heptazine imide) Salts. *Adv. Mater.* **2017**, *29*, 1700555.
(30) Savateev, A.; Pronkin, S.; Epping, J. D.; Willinger, M. G.; Wolff, C.; Neher, D.; Antonietti, M.; Dontsova, D. Potassium Poly(heptazine imides) from Aminotetrazoles: Shifting Band Gaps of Carbon Nitride-like Materials for More Efficient Solar Hydrogen and Oxygen Evolution. *ChemCatChem* **2017**, *9*, 167−174.
(31) Zhang, J.; Zhang, M.; Yang, C.; Wang, X. Nanospherical Carbon Nitride Frameworks with Sharp Edges Accelerating Charge Collection and Separation at a Soft Photocatalytic Interface. *Adv. Mater.* **2014**, *26*, 4121−4126.
(32) Yue, B.; Li, Q.; Iwai, H.; Kako, T.; Ye, J. Hydrogen production using zinc-doped carbon nitride catalyst irradiated with visible light. *Sci. Technol. Adv. Mater.* **2011**, *12*, No. 034401.
(33) Qiu, P.; Chen, H.; Xu, C.; Zhou, N.; Jiang, F.; Wang, X.; Fu, Y. Fabrication of an exfoliated graphitic carbon nitride as a highly active visible light photocatalyst. *J. Mater. Chem. A* **2015**, *3*, 24237−24244.
(34) Ayyub, M. M.; Chhetri, M.; Gupta, U.; Roy, A.; Rao, C. N. R. Photochemical and Photoelectrochemical Hydrogen Generation by Splitting Seawater. *Chem. − Eur. J.* **2018**, *24*, 18455−18462.
(35) Wang, Y.-L.; Mebel, A.; Wu, C.-J.; Chen, Y.-T.; Lin, C.-E.; Jiang, J.-C. IR spectroscopy and theoretical vibrational calculation of the melamine molecule. *J. Chem. Soc. Faraday Trans.* **1997**, *93*, 3445−3451.
(36) Jorge, A. B.; Martin, D. J.; Dhanoa, M. T. S.; Rahman, A. S.; Makwana, N.; Tang, J.; Sella, A.; Corà, F.; Firth, S.; Darr, J. A.; McMillan, P. F. H_2 and O_2 Evolution from Water Half-Splitting Reactions by Graphitic Carbon Nitride Materials. *J. Phys. Chem. C* **2013**, *117*, 7178−7185.
(37) Wu, W.; Guo, H.; Wu, W.; Ji, S.; Zhao, J. Long-Lived Room Temperature Deep-Red/Near-IR Emissive Intraligand Triplet Excited State (3IL) of Naphthalimide in Cyclometalated Platinum(II) Complexes and Its Application in Upconversion. *Inorg. Chem.* **2011**, *50*, 11446−11460.
(38) Wu, W.; Wu, W.; Ji, S.; Guo, H.; Zhao, J. Accessing the long-lived emissive 3IL triplet excited states of coumarin fluorophores by direct cyclometallation and its application for oxygen sensing and upconversion. *Dalton Trans.* **2011**, *40*, 5953−5963.
(39) Wu, W.; Wu, X.; Zhao, J.; Wu, M. Synergetic effect of C*N^N/C^N^N coordination and the arylacetylide ligands on the photophysical properties of cyclometalated platinum complexes. *J. Mater. Chem. C* **2015**, *3*, 2291−2301.
(40) Shalom, M.; Inal, S.; Fettkenhauer, C.; Neher, D.; Antonietti, M. Improving Carbon Nitride Photocatalysis by Supramolecular Preorganization of Monomers. *J. Am. Chem. Soc.* **2013**, *135*, 7118−7121.
(41) Xu, W.; An, X.; Zhang, Q.; Li, Z.; Zhang, Q.; Yao, Z.; Wang, X.; Wang, S.; Zheng, J.; Zhang, J.; Wu, W.; Wu, M. Cesium Salts as Mild Chemical Scissors To Trim Carbon Nitride for Photocatalytic H_2 Evolution. *ACS Sustainable Chem. Eng.* **2019**, *7*, 12351−12357.

https://dx.doi.org/10.1021/acsami.0c13060
ACS Appl. Mater. Interfaces 2020, 12, 48526−48532